PHYSICAL REVIEW D **92,** 094510 (2015)

Pion quasiparticle in the low-temperature phase of QCD

Bastian B. Brandt,[1] Anthony Francis,[2] Harvey B. Meyer,[3,4] and Daniel Robaina[3,*]

[1]*Institut für theoretische Physik, Universität Regensburg, D-93040 Regensburg, Germany*
[2]*Department of Physics & Astronomy, York University, 4700 Keele St, Toronto, Ontario M3J 1P3, Canada*
[3]*PRISMA Cluster of Excellence & Institut für Kernphysik, Johannes Gutenberg-Universität Mainz, D-55099 Mainz, Germany*
[4]*Helmholtz Institut Mainz, Johannes Gutenberg-Universität Mainz, D-55099 Mainz, Germany*

(Received 25 June 2015; published 10 November 2015)

We investigate the properties of the pion quasiparticle in the low-temperature phase of two-flavor QCD on the lattice with support from chiral effective theory. We find that the pion quasiparticle mass is significantly reduced compared to its value in the vacuum, in contrast with the static screening mass, which increases with temperature. By a simple argument, near the chiral limit the two masses are expected to determine the quasiparticle dispersion relation. Analyzing two-point functions of the axial charge density at nonvanishing spatial momentum, we find that the predicted dispersion relation and the residue of the pion pole are consistent with the lattice data at low momentum. This test, based on fits to the correlation functions, is confirmed by a second analysis using the Backus-Gilbert method.

DOI: 10.1103/PhysRevD.92.094510 PACS numbers: 12.38.Gc, 11.10.Wx, 12.39.Fe

I. INTRODUCTION

Identifying the spectrum of excitations of strongly interacting matter at finite temperature is of central importance to understanding the nature of the medium. These excitations are encoded as poles in thermal correlation functions. Weakly interacting probes coupling to local operators make it possible to measure the properties of these excitations experimentally, at least in principle. The prime example of such a probe is the photon. In practice, a medium is created in heavy-ion collisions which appears to reach thermal equilibrium locally, the temperature decreasing with time. Therefore a weighted average of thermal photon or dilepton spectra over the spacetime history of the "fireball" is obtained (see e.g. Refs. [1,2] and references therein).

In the low-temperature phase, it is natural to ask how close the properties of the excitations are to those of the known hadrons at zero temperature. Viewed globally, the spectrum does not appear to change much until temperatures close to the transition temperature are reached, where the rapid crossover to a deconfined and chirally symmetric phase takes place. This conclusion is based on the success of the hadron resonance gas model (HRG) in describing equilibrium properties of the medium (particularly the equation of state and quark number susceptibilities) computed in lattice QCD [3–5], and on its success in describing particle yields in heavy-ion collisions [6,7]. However, reliable information about individual excitations is sparse.

Here we extend our study [8] of the pion at finite temperature in two-flavor lattice QCD with support from a thermal chiral effective theory [9–11]. In Ref. [8] we performed a temperature scan on 16×32^3 ensembles; here we focus on one temperature ($T = 170$ MeV) on a fine lattice (24×64^3) with high statistics, for which we also have a reference zero-temperature ensemble at the same bare parameters.

At finite temperature it is important to distinguish between the pion static screening mass and the quasiparticle mass. The former is the inverse length scale over which a localized pseudoscalar perturbation turned on adiabatically is screened. It is thus a property of the static response of the system. The pion quasiparticle mass is a property of the dynamic response and can be given the following interpretation. Suppose that the expectation value of the axial charge is driven out of equilibrium adiabatically by an external perturbation until the instant $t = 0$, where the perturbation is switched off. Consider then how the system relaxes back to equilibrium at large positive times. The pion quasiparticle mass (times $c^2/\hbar$) is the frequency at which the axial charge present in the system would oscillate as a function of time.[1] Technically, while the quasiparticle mass is the real part of a pole of the retarded correlator $G_R(\omega, |\mathbf{p}| = 0)$ of the pseudoscalar density in the frequency variable, the static screening mass is a pole of $G_R(\omega = 0, \mathbf{p})$ in the spatial momentum $|\mathbf{p}|$. At zero temperature, Lorentz symmetry implies that the two masses are equal.

Our study shows that the zero-temperature pion mass "splits" at finite temperature into a lower pion quasiparticle mass and a higher pion screening mass,

*Corresponding author.
robaina@kph.uni-mainz.de

[1]The amplitude of the oscillations would be damped slowly in comparison with the oscillation frequency. The interpretation given is valid in the linear response approximation. By contrast, perturbing a conserved quark number (vector charge) with a wave vector $\mathbf{k}$ leads to a purely damped late-time response $e^{-D\mathbf{k}^2 t}$, where D is the diffusion coefficient.

$$T = 0: \qquad \text{pion mass} = 267(2)\ \text{MeV}$$
$$\swarrow \qquad \searrow$$
$$T = 169\ \text{MeV}: \quad \text{quasiparticle mass} = 223(4)\ \text{MeV} \qquad \text{screening mass} = 303(4)\ \text{MeV}$$

The pion quasiparticle mass can be extracted model independently near the chiral limit due to the dominance of its contribution to the two-point function of the axial-charge density and of the pseudoscalar density. In contrast to the mass, we find that the decay constant associated with the pion quasiparticle practically retains its zero-temperature value.

It may seem surprising that the thermal quasiparticle mass differs substantially from the zero-temperature mass, given that the hadron resonance gas model works well for equilibrium properties, and that the model assumes an unmodified spectrum of excitations corresponding to the well-known $T = 0$ hadrons. Some comments on this apparent contradiction are made in the conclusion.

By a simple argument, the dispersion relation of the pion at low momenta is given by a single parameter u [see Eq. (11) below], which in the chiral limit corresponds to the group velocity of the excitation. As in Ref. [8], we determine this parameter as the ratio of the quasiparticle mass to the screening mass, $u \approx 0.74$. As a new aspect, we then test whether the so-determined parameter u correctly predicts the momentum dependence of the pion energy by looking at the two-point function of the axial-charge density at nonvanishing spatial momentum. An important observation is that the chiral Ward identities also predict the residue of the pion pole in the axial-current two-point functions. Due to the difficulty of extracting real-time information from Euclidean correlation functions, testing simultaneously the predictions for the pole and the residue proves to be essential to improve the discriminative power of the analysis. Since the chiral predictions are only expected to be valid at sufficiently small momenta, we also provide an estimate of the range of validity of the effective theory.

Our analysis method of lattice correlation functions is based on fits, where the *ansatz* is motivated by the chiral effective theory at small frequencies and on perturbation theory at high frequency. We also present an alternative analysis, which starts by generating model independently a locally averaged spectral function by following the Backus-Gilbert inversion method [12–17]. In a second step, a pion pole contribution with the predicted dispersion relation is assumed, allowing us to obtain an estimate for the residue. The advantage of this alternative analysis is that we do not have to formulate an explicit *ansatz* for the spectral density of the non-pion contributions. This point is particularly relevant since at finite spatial momentum, axial-vector excitations do contribute to the two-point function of the axial-charge density.

The paper is organized as follows. Section II contains an overview of the theory expectations concerning the two-point functions of the axial current at finite temperature. Sections III and IV present the lattice QCD calculation, and our conclusions are given in Sec. V. In Appendix A, the tensor structure of the axial-current two-point functions at finite temperature is given; in Appendix B, we derive the contribution of the pion to the four independent tensor structures, thus determining all the relevant residues; in Appendix C we perform a mock-data study of the Backus-Gilbert method. Finally, Appendix D contains Table VII with the lattice correlator data.

II. THEORY BACKGROUND

We work in the Euclidean path-integral formalism, and our notation and conventions follow those used in Ref. [8]. The vector and axial-vector currents and the pseudoscalar density are given by

$$V_\mu^a(x) = \bar\psi(x)\gamma_\mu \frac{\tau^a}{2}\psi(x), \qquad A_\mu^a(x) = \bar\psi(x)\gamma_\mu\gamma_5 \frac{\tau^a}{2}\psi(x),$$
$$P^a(x) = \bar\psi(x)\gamma_5 \frac{\tau^a}{2}\psi(x), \tag{1}$$

where ψ is the isospin-doublet quark field. In Appendix A, we provide a decomposition in momentum space of the Lorentz structure of the two-point functions of the axial current. For a general momentum p, they are entirely described by four "form factors," which in the rest frame of the thermal medium are functions of p_0 and $\mathbf{p}^2$. At zero temperature, the four functions reduce to two functions of p^2, one longitudinal and one transverse. The partially conserved axial-current (PCAC) relation relates the two-point function $\langle P^a(x)P^b(0)\rangle$ of the pseudoscalar density, as well as the $\langle A_\mu^a(x)P^b(0)\rangle$ correlation functions to the aforementioned form factors.

In this work, we investigate the following static screening correlators:

$$\delta^{ab} G_A^s(x_3, T) = \int dx_0 d^2x_\perp \langle A_3^a(x) A_3^b(0)\rangle, \tag{2}$$

$$\delta^{ab} G_P^s(x_3, T) = \int dx_0 d^2x_\perp \langle P^a(x) P^b(0)\rangle, \tag{3}$$

where $x_\perp = (x_1, x_2)$. Time-dependent correlators with a general spatial momentum $\mathbf{p}$ will also play a crucial role,

$$\delta^{ab}G_A(x_0,T,\mathbf{p}) = \int d^3x e^{i\mathbf{p}\cdot\mathbf{x}}\langle A_0^a(x)A_0^b(0)\rangle, \quad (4)$$

$$\delta^{ab}G_P(x_0,T,\mathbf{p}) = \int d^3x e^{i\mathbf{p}\cdot\mathbf{x}}\langle P^a(x)P^b(0)\rangle. \quad (5)$$

They are related by Fourier transformations to the form factors defined in Appendix A, for instance

$$G_A^{\mathrm{s}}(x_3,T) = \int \frac{dp_3}{2\pi} e^{-ip_3x_3}\Pi^{\mathrm{L,l}}(0,p_3^2). \quad (6)$$

The correlators $G_A(x_0,T,\mathbf{0})$ and $G_A^{\mathrm{s}}(x_3,T)$ are only sensitive to the longitudinal form factor $\Pi^{\mathrm{L,l}}$; these were the cases considered in Ref. [8]. At nonvanishing momentum however, the correlator $G_A(x_0,T,\mathbf{p})$ is sensitive to three independent form factors $\Pi^{\mathrm{T,l}}$, Π^{M} and $\Pi^{\mathrm{L,l}}$.

At long distances, the screening correlator $G_A^{\mathrm{s}}(x_3,T)$ is given by

$$G_A^{\mathrm{s}}(x_3,T) \overset{|x_3|\to\infty}{=} \frac{1}{2} f_\pi^2 m_\pi e^{-m_\pi|x_3|}, \quad (7)$$

which defines the screening pion mass m_π and the associated decay constant[2] f_π. The Gell-Mann–Oakes–Renner relation

$$f_\pi^2 m_\pi^2 = -m\langle\bar{\psi}\psi\rangle \quad (8)$$

holds to leading order in the chiral expansion. From Eqs. (6) and (7), the low-momentum analytic structure of the longitudinal form factor $\Pi^{\mathrm{L,l}}$ reads

$$\Pi^{\mathrm{L,l}}(0,\mathbf{p}^2) = \frac{f_\pi^2 m_\pi^2}{\mathbf{p}^2+m_\pi^2}, \qquad \mathbf{p}\to 0. \quad (9)$$

More generally, expanding the denominator in the frequency,

$$\mathbf{p}^2 + m_\pi^2 \to \mathbf{p}^2 + m_\pi^2 + \frac{1}{u^2}\omega_n^2 + \cdots, \quad (10)$$

it follows that a quasiparticle (pole in the retarded correlator as a function of frequency) with the dispersion relation [10,11]

$$\omega_{\mathbf{p}} = u(T)\sqrt{m_\pi^2+\mathbf{p}^2} \quad (11)$$

exists at low momenta.[3] The remarkable aspect is that the parameter u determines both the (real part of the) dispersion relation of the quasiparticle and the ratio of the quasiparticle mass to the screening mass. A graphical interpretation of the dual role of the parameter u is given in Fig. 1. Here the trajectory in the frequency-momentum plane of a pole in the retarded correlator of the pseudoscalar density[4] corresponds to a static screening state at $\mathbf{p}^2=-m_\pi^2$, and to a real-time quasiparticle at small positive $\mathbf{p}^2$. In Ref. [8], the parameter u was determined using lattice correlation functions at vanishing spatial momentum via the two estimators

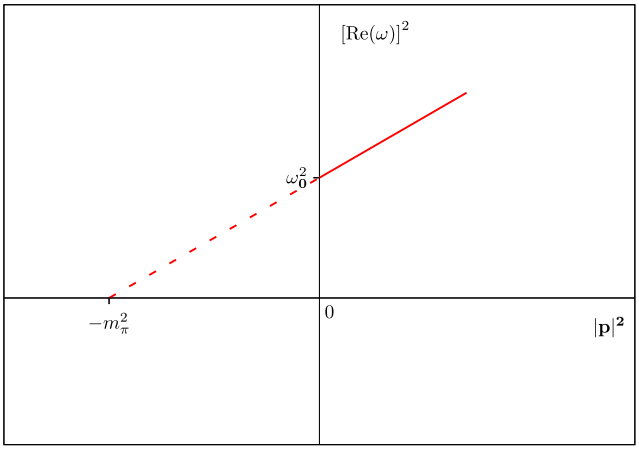

FIG. 1 (color online). Trajectory in the $(\omega,\mathbf{p})$ plane of the pion pole in the pseudoscalar retarded correlator. At negative $\mathbf{p}^2$ the pole corresponds to the pion screening mass, while at positive $\mathbf{p}^2$ it corresponds to the pion quasiparticle. The slope is the value of $u^2(T)$.

$$u_m = \left[-\frac{4m_q^2}{m_\pi^2}\frac{G_P(x_0,T,0)}{G_A(x_0,T,0)}\bigg|_{x_0=\beta/2}\right]^{1/2}, \quad (12)$$

$$u_f = \frac{f_\pi^2 m_\pi}{2G_A(\beta/2,T,0)\sinh(u_f m_\pi\beta/2)}. \quad (13)$$

In doing so, the parametric dominance of the pion in the time-dependent Euclidean correlator at small quark masses is exploited. Good agreement was found between u_f and u_m at $T\simeq 150$ MeV for a zero-temperature pion mass of 305 MeV. Any departure of u from unity clearly represents a breaking of Lorentz invariance due to thermal effects. In this work, one of our goals is to test whether the parameter u determined from the ratio of the quasiparticle to the screening mass, as in Ref. [18], really does predict the dispersion relation of the quasiparticle, as in Eq. (11). In order to reach this goal, we perform an analysis of the time-dependent Euclidean correlator $G_A(x_0,T,\mathbf{p})$ in terms of the spectral function ρ^A. They are related as follows:

[2]The normalization convention is such that at zero temperature $f_\pi\approx 92$ MeV.

[3]In this argument, the imaginary part of the frequency pole is neglected. A more sophisticated argument is required to show that the damping rate of the pion quasiparticle is indeed parametrically subleading [11].

[4]Recall that the momentum-space Euclidean correlator $G_E(\omega_n,\mathbf{p})$ is related to the retarded correlator via $G_R(i\omega_n,\mathbf{p}) = G_E(\omega_n,\mathbf{p})$ for $\omega_n\geq 0$ [18].

$$G_A(x_0,T,\mathbf{p}) = \int_0^\infty d\omega \rho^A(\omega,\mathbf{p}) \frac{\cosh(\omega(\beta/2-x_0))}{\sinh(\omega\beta/2)}. \tag{14}$$

First we recall that at zero temperature, the Lorentz structure of the axial-current two-point function implies the following momentum dependence of the pion pole contribution:

$$G_A(x_0,T=0,\mathbf{p}) \overset{|x_0|\to\infty}{\sim} \mathrm{Res}(\omega^0_{\mathbf{p}}) \frac{e^{-\omega^0_{\mathbf{p}}|x_0|}}{2\omega^0_{\mathbf{p}}} \tag{15}$$

where the residue is here given by

$$\mathrm{Res}(\omega^0_{\mathbf{p}}) = (f^0_\pi \omega^0_{\mathbf{p}})^2, \qquad \omega^0_{\mathbf{p}} = (\mathbf{p}^2 + (\omega^0_{\mathbf{0}})^2)^{1/2}. \tag{16}$$

In terms of the spectral functions, this correlator corresponds to

$$\rho^A(\omega,T=0,\mathbf{p}) = \mathrm{Res}(\omega^0_{\mathbf{p}})\delta(\omega^2-(\omega^0_{\mathbf{p}})^2) + \cdots. \tag{17}$$

At the other end of the spectrum, in the high-frequency region, a leading-order perturbative calculation (see for instance Ref. [19]) yields

$$\rho^A(\omega,T,\mathbf{p}) = \theta(\omega^2-4m^2-\mathbf{p}^2)\frac{N_c}{24\pi^2}(\mathbf{p}^2+6m^2), \quad \omega\to\infty. \tag{18}$$

We note that at nonzero momentum, the correlator $G_A(x_0,T=0,\mathbf{p})$ receives contributions from axial-vector mesons via the transverse form factor (see Appendix A),

$$G_A(x_0,T=0,\mathbf{p}) = \int \frac{dp_0}{2\pi} e^{-ip_0x_0}\left[\frac{\mathbf{p}^2}{p_0^2+\mathbf{p}^2}\Pi^{\mathrm{T}}(p_0^2+\mathbf{p}^2) + \frac{{p_0}^2}{p_0^2+\mathbf{p}^2}\Pi^{\mathrm{L}}(p_0^2+\mathbf{p}^2)\right]. \tag{19}$$

The spectral functions associated with the form factors Π^{T} and Π^{L} are measured experimentally in τ decays [20]. The most prominent excitation in the transverse spectral function is the $a_1(1260)$ meson, while the longitudinal spectral function is dominated by the pion. Since Π^{T} describes by itself the two-point function of spatial components of the axial current at vanishing spatial momentum, it cannot contain the pion pole. The latter is entirely contained in the form factor Π^{L}.

At finite temperature, the pion pole appears in all three form factors contributing to $G_A(x_0,T,\mathbf{p})$; they are given explicitly in Appendix A. In the limit $T\to 0$, one of the three form factors turns into Π^{T}, one turns into Π^{L} and the third one vanishes (Appendix A 2). Therefore the pion contribution to the first form factor must vanish in the limit $T\to 0$, in view of the remarks above, and indeed, we find it to be proportional to $(1-u^2)$ [recall that $\lim_{T\to 0}u(T)=1$ by Lorentz symmetry]. Altogether, the pion contribution to the spectral function ρ^A is predicted to have the form $\rho^A(\omega,T,\mathbf{p}) = \mathrm{Res}(\omega_{\mathbf{p}})\delta(\omega^2-\omega^2_{\mathbf{p}})$, with the dispersion relation given by Eq. (11) and the residue by (see Appendix B)

$$\mathrm{Res}(\omega_{\mathbf{p}}) = f_\pi^2(m_\pi^2+\mathbf{p}^2). \tag{20}$$

For later use we also define the pion quasiparticle decay constant f^t_π via

$$\mathrm{Res}(\omega_{\mathbf{0}}) = (f^t_\pi \omega_{\mathbf{0}})^2. \tag{21}$$

The contribution to the Euclidean correlator then reads

$$G_A(x_0,T,\mathbf{p}) = \frac{\mathrm{Res}(\omega_{\mathbf{p}})}{2\omega_{\mathbf{p}}}\frac{\cosh(\omega_{\mathbf{p}}(\beta/2-x_0))}{\sinh(\omega_{\mathbf{p}}\beta/2)} + \cdots. \tag{22}$$

Whether the residue determined through fits to lattice correlation functions agrees with Eq. (20) provides a cross-check that the low-energy effective description is working.

III. LATTICE SETUP

In this section we describe the analysis performed on a finite-temperature ensemble of size 24×64^3 with two degenerate dynamical light flavors. The short direction is interpreted as time and therefore the temperature is $T = 1/24a = 169(3)$ MeV while the spatial extent amounts to $L = 64a = 3.1$ fm. The fields admit thermal boundary conditions in time and periodic boundary conditions in space. We use the Wilson plaquette action [21] and the O(a)-improved Wilson fermion action with a nonperturbatively determined c_{sw} coefficient [22]. The configurations were generated using the MP-HMC algorithm [23] following the implementation described in Ref. [24] based on Lüsher's DD-HMC package [25]. In addition, we use a 128×64^3, effectively zero-temperature ensemble that was made available to us through the Coordinated Lattice Simulations (CLS) effort (labelled as O7 in Ref. [26]) with all bare parameters identical to our finite-temperature ensemble. The pion mass takes a value of $m_\pi = 270$ MeV [26] such that $m_\pi L = 4.2$. This additional zero-temperature test ensemble allows us to compare thermal observables in a straightforward manner with their corresponding "effective zero-temperature" value calculated in the O7 ensemble.

A. PCAC mass

In order to check that our thermal ensemble indeed yields the same physical quark mass as its corresponding zero-temperature counterpart (O7), we use the definition of the

quark mass based on the PCAC (partially conserved axial current) relation [27,28]

$$m_{\mathrm{PCAC}}(x_3) = \frac{1}{2}\frac{\int dx_0 d^2x_\perp \langle \partial_3^{\mathrm{imp}} A_3^{\mathrm{imp}}(x) P(0)\rangle}{\int dx_0 d^2x_\perp \langle P(x)P(0)\rangle}, \quad x_\perp = (x_1, x_2) \tag{23}$$

where in the improvement process

$$A_\mu^a \to A_\mu^{\mathrm{imp},a} = A_\mu^a + a c_A \partial_\mu^{\mathrm{imp}} P^a. \tag{24}$$

The derivative $\partial_\mu^{\mathrm{imp}}$ is the improved lattice discretized version of the derivative following Ref. [29]. The nonperturbatively calculated coefficient c_A was taken from Ref. [30]. Note that since Eq. (23) stems from an operator identity, we are free to choose the direction of measurement. On the thermal ensemble, the spatial directions are longer; therefore, by measuring along these directions we obtain a longer plateau and thus more accurate determinations of the PCAC mass. The extraction can be carried out by performing a fit to a constant in the range where a plateau is observed (see Fig. 2). Its central value and error, given in Table I, are in very good agreement with the ones quoted in Ref. [31].

B. Pseudoscalar and axial-vector correlators

Our goal is to calculate the temperature-dependent coefficient $u(T)$ that parametrizes the pion dispersion relation (11). In Ref. [8], we defined two estimators u_f and u_m that yielded consistent results up to $T \simeq 170$ MeV for the case of two degenerate light flavors with $\bar{m}^{\overline{\mathrm{MS}}}(\mu = 2\ \mathrm{GeV}) \sim 15$ MeV; at that quark mass, the crossover region is located around $T_C \simeq 211$ MeV [32]. In the thermal ensemble we are analyzing here, we have $\bar{m}^{\overline{\mathrm{MS}}}(\mu = 2\ \mathrm{GeV}) = 12.8(1)$ MeV (see Table I), and therefore expect a slightly lower value of the transition temperature. Nevertheless, this should not affect the applicability of the chiral expansion around $(T, m = 0)$ with $T < T_C$, as discussed in Ref. [8].

We use the correlators defined in Eqs. (2)–(5) with the spatial momenta given by

$$\mathbf{p} = \mathbf{p}_n \equiv (0, 0, 2\pi n/L). \tag{25}$$

The improvement of the axial current was already introduced in Eq. (24). Note that since all two-point functions belong to the adjoint (or *isovector*) representation of $\mathrm{SU}(N_f)$ ($N_f = 2$), the contributions of quark disconnected diagrams cancel out. The renormalization program is carried out such that

$$G_A(x_0, T, \mathbf{p}) = (Z_A(g_0^2))^2 G_A(x_0, g_0^2, T, \mathbf{p}), \tag{26}$$

$$G_P(x_0, T, \mathbf{p}) = (Z_P(g_0^2))^2 G_P(x_0, g_0^2, T, \mathbf{p}) \tag{27}$$

and similarly for the screening correlators; the value of the coefficients Z_A and Z_P can be found in Table I.

TABLE I. Summary of the main parameters for the 24×64^3 finite-temperature ensemble as well as for the 128×64^3 zero-temperature ensemble labeled as O7 in Ref. [26]. The quark mass is computed at and normalized with the $T = 1/24a$ temperature. The statistics collected for two-point functions are respectively 360 and 149 configurations at $N_\tau = 24$ and $N_\tau = 128$, with respectively 64 and 16 point sources per configuration, exploiting the translational invariance of the system.

$6/g_0^2$	5.50
κ	0.13671
c_{sw}	1.751496
$T_{N_\tau=24}$ [MeV]	169(3)
$T_{N_\tau=128}$ [MeV]	32(1)
a [fm] [26]	0.0486(4)(5)
Z_A [26]	0.793(4)
Z_P [26]	0.5184(53)
$\bar{m}^{\overline{\mathrm{MS}}}/T(\mu = 2\ \mathrm{GeV})$	0.0757(7)

IV. ANALYSIS OF LATTICE TWO-POINT FUNCTIONS

After the preliminary work presented in the previous section, we turn to the analysis of correlation functions in order to extract the pion properties.

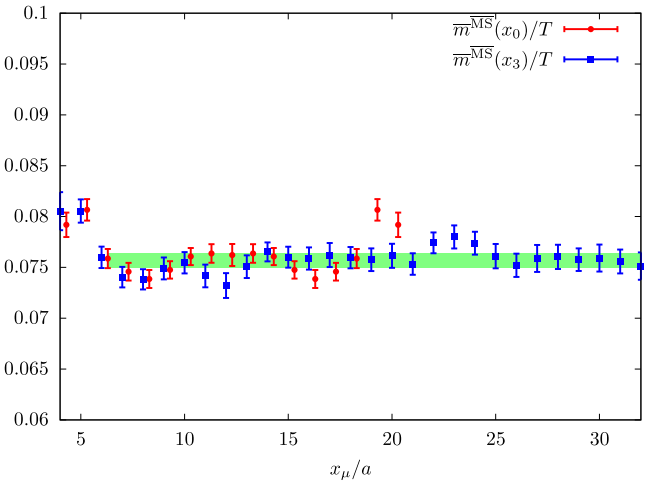

FIG. 2 (color online). The PCAC masses. The renormalization factors Z_A and Z_P are included, as well as the conversion factor from the Schrödinger Functional (SF) to the Minimal Subtraction ($\overline{\mathrm{MS}}$) scheme at a scale of $\mu = 2$ GeV, which amounts to 0.968 (20) [26]. We also plot the result along the x_0 direction to show that indeed both are compatible. This can be interpreted as a check that cutoff effects are indeed small for this value of the lattice spacing.

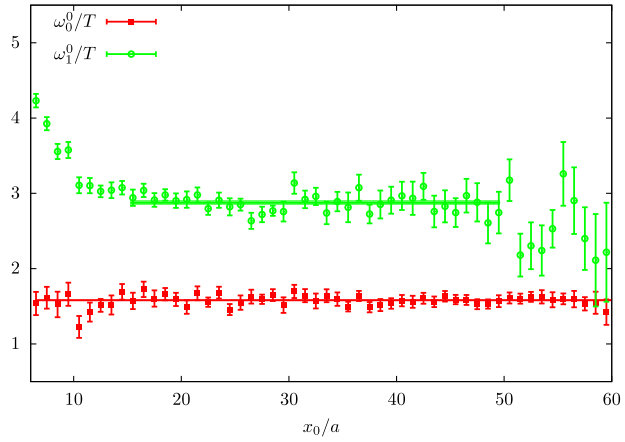

FIG. 3 (color online). Effective "cosh" masses for the O7 zero-temperature ensemble in the $\langle A_0 A_0 \rangle$ channel for $n = 0$, 1. The values of $\omega_n^0 \equiv \omega_{\mathbf{p}_n}^0$ are given in units of the temperature $T = 1/24a$ corresponding to our thermal ensemble.

A. The zero-temperature case

As a benchmark we analyze zero-temperature data on the O7 ensemble. Here we are able to obtain the pion energy $\omega_{\mathbf{p}}^0$ by fitting a constant to the effective mass. The pion energy corresponding to $\mathbf{p} = 0$ and $\mathbf{p} = (0, 0, 2\pi/L)$ can be read off from the plot in Fig. 3. The dominance of the pion contribution, particularly in the zero-momentum case, is clearly very strong. Performing a linear fit to $(\omega_{\mathbf{p}}^0)^2$ as a function of $\mathbf{p}^2$, we obtain for the slope $u^2(T \simeq 0) = 1.01(6)$, consistently with Lorentz invariance. The decay constant f_π^0, defined by Eq. (16), indeed turns out to be independent of the momentum.

Once the ground state dominates the correlator $G_A(x_0, T \simeq 0, \mathbf{p})$, one-state cosh fits of the form $A_1 \cosh(\omega_{\mathbf{p}}^0(T/2 - x_0))$ with $T = 128a$ are applied and the results are summarized in Table II. The values for $\omega_{\mathbf{0}}^0$ and f_π^0 are in very good agreement with the ones quoted in Ref. [31].

TABLE II. Properties of the pion at zero temperature. The index n denotes the momentum $\mathbf{p}_n$ induced and $\omega_{\mathbf{p}_n}^0$ corresponds to the energy of the state (in particular, $\omega_{\mathbf{0}}^0$ is the pion mass). All errors are purely statistical, and all renormalization factors are included. The fit interval begins at $x_0/a = 6$ for the zero-momentum case and at $x_0/a = 15$ for one unit of momentum in view of the effective mass plot of Fig. 3. Dimensionful quantities are normalized with $T = 1/24a$.

n	A_1/T^3	$\omega_{\mathbf{p}_n}^0/T$	χ^2/d.o.f	f_π^0/T	Res($\omega_{\mathbf{p}}$)
0	$8.4(3) \times 10^{-3}$	1.579(12)	0.05	0.599(8)	0.89(3)
1	$5.3(4) \times 10^{-4}$	2.88(3)	0.4	0.629(12)	3.27(15)

B. The screening quantities f_π and m_π at finite temperature

A detailed description of how the extraction is carried out can be found in Ref. [8]. Here, we highlight the basic relations that lead to the extraction of the screening quantities f_π and m_π and therefore to the values of the estimators u_f and u_m.

(i) The screening mass m_π is calculated by fitting the correlation function $G_P^{\mathrm{s}}(x_3, T)$ with a two-state *ansatz* of the form $\sum_{i=1}^{2} A_i \cosh[m_i(L/2 - x_3)]$ with masses m_i and amplitudes A_i. The value obtained for the ground-state mass is compatible with the value obtained from the "cosh" mass which is defined as the positive root of the following equation (see Fig. 4):

$$\frac{G_P^{\mathrm{s}}(x_3, T)}{G_P^{\mathrm{s}}(x_3 + a, T)} = \frac{\cosh[m_{\cosh}(x_3 + a/2)(x_3 - L/2)]}{\cosh[m_{\cosh}(x_3 + a/2)(x_3 + a - L/2)]}. \tag{28}$$

(ii) We determine the screening pion decay constant from the correlator $G_A^{\mathrm{s}}(x_3, T)$ via Eq. (7) by applying again a two-state "cosh" *ansatz*. The screening pion mass m_π also appears in G_A^{s}. We use this fact as a consistency check, but due to the better signal-to-noise ratio of the pseudoscalar channel, we quote the value extracted from G_P^{s} as our final result for m_π.

C. Thermal time-dependent correlators at zero momentum

The estimators u_f and u_m for the pion velocity u are defined in Eqs. (12)–(13). Apart from the PCAC mass, f_π and m_π, they involve the time-dependent correlators $G_A(x_0, T, \mathbf{0})$ and $G_P(x_0, T, \mathbf{0})$. The difference between u_f

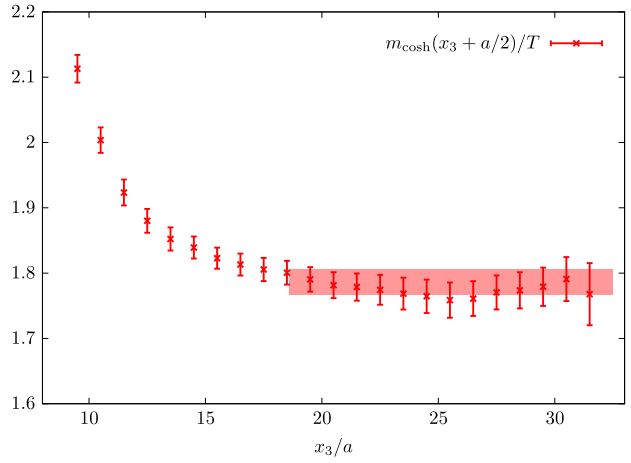

FIG. 4 (color online). Effective "cosh" mass plot for the screening mass m_π. The plateau has been chosen to begin at $x_3/a = 19$.

TABLE III. Summary of the results for the $N_\tau = 24$ thermal ensemble. All renormalization factors are included and the errors are purely statistical. The value of $\omega_{\mathbf{0}}$ is calculated using $\omega_{\mathbf{0}} = u_m m_\pi$. In the same way $f_\pi^t = f_\pi/u_m$. The value of the residue is obtained according to Eq. (20), $\mathrm{Res}(\omega_{\mathbf{0}}) = f_\pi^2 m_\pi^2$.

m_π/T	1.79(2)
f_π/T	0.46(1)
u_f	0.76(1)
u_m	0.74(1)
u_f/u_m	1.02(1)
$\omega_{\mathbf{0}}/T$	1.32(2)
f_π^t/T	0.62(1)
$\mathrm{Res}(\omega_{\mathbf{0}})/T^4$	0.68(2)

and u_m can be explained as follows. The estimator u_m is based on the dominance of the pion contribution in the correlators G_A and G_P at $x_0 = \beta/2$; the estimator u_f is based on assuming that the residue is given by the screening quantities (as predicted by the chiral effective theory), $\mathrm{Res}(\omega_{\mathbf{0}}) = f_\pi^2 m_\pi^2$, and the dominance of the pion contribution in G_A only. The dominance in G_A is less strong an assumption than the assumption that the pion dominates G_P, since their spectral functions are related by $\rho_P(\omega) = -\frac{\omega^2}{4m^2}\rho_A(\omega)$ at zero spatial momentum. We summarize results for u_f and u_m in Table III.

The chiral expansion around $(T, m = 0)$ proposed in Ref. [11] assumes that one is sufficiently close to the chiral limit. In this limit, the screening pion mass m_π vanishes and the coefficient $u(T)$ is indeed the velocity of a massless pion quasiparticle in the presence of a thermal bath. A deviation from unity corresponds to a violation of boost invariance. At finite but small quark mass, we showed in Ref. [8] that the consistency of u_f and u_m serves as an indicator for the applicability of the chiral expansion. Based on the results of Table III, we conclude that they are indeed consistent. The results, in particular for u_f, are in good agreement with the results obtained in Ref. [8] on ensembles with a coarser lattice spacing and a slightly heavier quark mass. Note that to leading order, u is expected to be independent of the quark mass.

The "reconstructed" correlator G_A^{rec} is defined as the thermal Euclidean correlator that would be realized if the spectral function remained the zero-temperature one. We compute it following the method first proposed in Ref. [33]. Figure 5 shows the difference between the thermal correlator and the reconstructed correlator. There is a statistically significant difference between the two correlators, which shows that a change must take place in the spectral function. Because the difference is very weakly dependent on time, the change must take place in the low-frequency part of the spectral function. We expect from the thermal chiral effective theory that the change is due to a modification of the mass and/or the residue of the pion

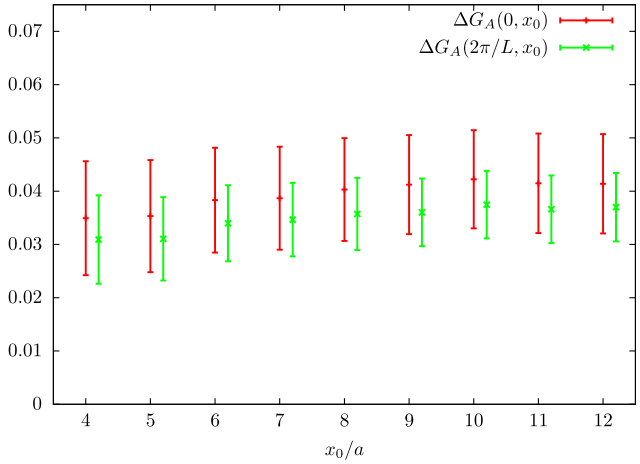

FIG. 5 (color online). The difference $\Delta G_A(|\mathbf{p}|, x_0) \equiv [G_A(x_0, T, \mathbf{p}) - G_A^{\mathrm{rec}}(x_0, T, \mathbf{p})]/T^3$ of the thermal correlator and the reconstructed correlator for $|\mathbf{p}| = 0$ and $2\pi/L$.

quasiparticle. Using the numbers of Table III, the changes amount respectively to

$$\frac{\omega_{\mathbf{0}}}{\omega_{\mathbf{0}}^0} = 0.836(14), \qquad \frac{f_\pi^t}{f_\pi^0} = 1.03(2). \tag{29}$$

We thus observe that while the pion decay constant remains unchanged at the precision level of a few percent, the pion mass decreases by 16%. Qualitatively, these results are consistent with the two-loop results in zero-temperature chiral perturbation theory given in Refs. [34,35]. Future lattice calculations approaching the chiral limit would allow for a quantitative comparison.

D. The spectral function $\rho^A(\omega, p)$ at nonzero momentum

As the next step, we test the functional form of Eq. (11) at nonzero momentum. The relevant real-time pion states with energy $\omega_{\mathbf{p}}$ have a nonzero overlap with the operator $\int d^3x e^{i\mathbf{px}} A_0(x)$; furthermore, the spectral function ρ_A becomes independent of ω in the ultraviolet, rather than growing like ω^2. We therefore expect to have the best sensitivity to the pion contribution in the correlator $G_A(x_0, T, \mathbf{p})$.

At finite temperature, the analysis of the correlator $G_A(x_0, T, \mathbf{p})$ is more involved than at zero temperature: only at sufficiently small quark masses and momenta, and not too small x_0 is the correlator parametrically dominated by the pion pole. Therefore we proceed by formulating a fit *ansatz* to take into account the non-pion contributions. The combination of Eqs. (17) and (18) motivates an *ansatz* for the spectral function reading

$$\rho^A(\omega, \mathbf{p}) = A_1(\mathbf{p}) \sinh(\omega\beta/2)\delta(\omega - \omega_{\mathbf{p}}) + A_2(\mathbf{p}) \frac{N_c}{24\pi^2}(1 - e^{-\omega\beta})\theta(\omega - c). \tag{30}$$

TABLE IV. Results of fits to the axial-charge density correlator at nonvanishing momentum $\mathbf{p}_n$. All errors quoted are statistical, and all renormalization factors are included. The quantity $\omega_{\mathbf{p}}/T$ is not a fit parameter; rather it is set to the value predicted by Eq. (11) with $u(T) = u_m = 0.74(1)$.

n	A_1/T^3	$\omega_{\mathbf{p}_n}/T$	$\tilde{A}_2$	c/T	$\mathrm{Res}(\omega_{\mathbf{p}_n})/T^4$	b	χ^2/d.o.f.
1	$2.95(4) \times 10^{-1}$	2.19(3)	1.78(8)	6.7(3)	1.72(6)	−0.08(3)	0.06
2	$1.40(5) \times 10^{-1}$	3.73(6)	1.26(2)	6.1(1)	3.3(2)	−0.39(4)	0.15
3	$4.9(3) \times 10^{-2}$	5.40(9)	1.19(1)	7.7(1)	3.9(5)	−0.65(4)	0.35
4	$1.7(2) \times 10^{-2}$	7.1(1)	1.15(1)	9.67(9)	4.21(7)	−0.78(3)	0.49
5	$4(1) \times 10^{-3}$	8.8(1)	1.12(1)	11.7(1)	3(1)	−0.89(3)	1.04

The corresponding form of the correlation function then reads

$$G^A(x_0, T, \mathbf{p}) = A_1(\mathbf{p}) \cosh(\omega_{\mathbf{p}}(\beta/2 - x_0)) + A_2(\mathbf{p}) \frac{N_c}{24\pi^2} \left(\frac{e^{-cx_0}}{x_0} + \frac{e^{-c(\beta - x_0)}}{\beta - x_0} \right). \quad (31)$$

We fit $G_A(x_0, T, \mathbf{p})$ with the *ansatz* given in Eq. (31) for the momenta $\mathbf{p}_n = (0, 0, 2\pi n/L)$ with $n = 1, 2, 3, 4, 5$. The fit interval is chosen to be $x_0/a \in [5, 12]$ in order to avoid cutoff effects. There are four parameters involved, $A_1(\mathbf{p})$, $\omega_{\mathbf{p}}$, $A_2(\mathbf{p})$ and c. Leaving $\omega_{\mathbf{p}}$ as a fit parameter led to poorly constrained fits. Therefore we set the value of $\omega_{\mathbf{p}}$ to the prediction of Eq. (11) in order to test whether the data can be described in this way. Motivated by the expected large-ω behavior of the spectral function, we quote the rescaled parameter $\tilde{A}_2 = A_2/\mathbf{p}^2$. Note that the quark mass is negligible compared to all the nonvanishing $|\mathbf{p}|$ values considered here. The expected value of $\tilde{A}_2$ is of order unity, in view of Eq. (18). Equation (22) allows us to establish the relation between the fit parameter $A_1(\mathbf{p})$ and the residue itself,

$$\mathrm{Res}(\omega_{\mathbf{p}}) = 2A_1(\mathbf{p})\omega_{\mathbf{p}} \sinh(\omega_{\mathbf{p}}\beta/2). \quad (32)$$

One may further convert the result for the residue into a parameter $b(\mathbf{p})$, defined by

$$\mathrm{Res}(\omega_{\mathbf{p}}) = f_\pi^2(m_\pi^2 + \mathbf{p}^2)(1 + b(\mathbf{p})). \quad (33)$$

From the chiral prediction (20), we thus expect $b(\mathbf{p})$ to be small compared to unity if the effective description is working. The results are summarized in Table IV.

The fits provide a good description of the data; see the χ^2/d.o.f. values and Fig. 6. We observe that at the smallest momentum, $|\mathbf{p}| \simeq 400$ MeV, $b(\mathbf{p})$ really is small, pointing to a successful check of the chiral prediction. At higher momenta, the negative, order-unity value of $b(\mathbf{p})$ indicates that the residue of the pion pole is reduced. It should also be remembered that at higher momenta, neglecting the width of the quasiparticle is bound to be an increasingly poor approximation. The coefficient $\tilde{A}_2$ is expected to be of order unity from the tree-level prediction (18). Indeed the numbers in Table IV are of order unity. One reason for the relatively large value of the coefficient at the smallest momentum could be that axial-vector excitations are contributing around the threshold c, thus adding spectral weight. The value of the threshold at $|\mathbf{p}| \simeq 400$ MeV, is about 1.1 GeV, a value we consider to be reasonable given that the mass of the lightest axial-vector meson in nature is $m_{a_1} \approx 1.2$ GeV.

In order to gauge the discriminative power of the test, it is interesting to ask whether a rather different model is consistent with the lattice data on $G_A(x_0, \mathbf{p}, T)$. We assume for this purpose that the dispersion relation and the residue have the same $\mathbf{p}$ dependence as at zero temperature. We therefore set $\omega_{\mathbf{p}} = \sqrt{\omega_{\mathbf{0}}^2 + \mathbf{p}^2}$, and obtain for $n = 1$ an equally good description of the data, with a value of the residue $\mathrm{Res}(\omega_{\mathbf{p}}) = 3.01(4)$ not too different from $(f_\pi^t)^2(\omega_{\mathbf{0}}^2 + \mathbf{p}^2) = 2.84(7)$. The other fit parameters take the values $\tilde{A}_2 = 2.42(17)$ and $c/T = 10.2(4)$. While the perturbative coefficient and the threshold values seem less

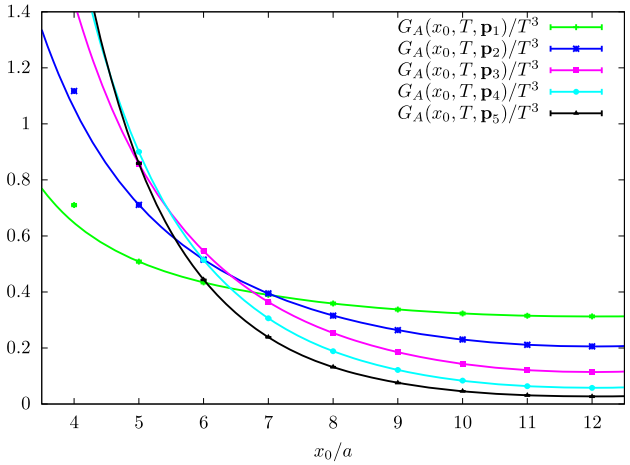

FIG. 6 (color online). Correlation functions $G_A(x_0, T, \mathbf{p}_n)/T^3$ with $\mathbf{p}_n = (0, 0, 2\pi n/L)$, together with the fits resulting from the four-parameter *ansatz* of Eq. (31). The corresponding parameter values are given in Table IV. All renormalization constants are included.

plausible to us, we cannot completely exclude this model on the basis of the lattice data.

To summarize, we have found that the dispersion relation of the pion quasiparticle is consistent with Eq. (11), the parameter u being determined at vanishing spatial momentum. In order to test the dependence of our results on the fit *ansatz* made, in the next section we apply the Backus-Gilbert method.

E. The Backus-Gilbert method for $\rho^A(\omega,\mathbf{p})$

The Backus-Gilbert method is a method suitable for inverting integral equations like Eq. (14). It has been studied in many contexts (see e.g. Refs. [12–17]). While it has not been applied in lattice QCD, to our knowledge, the central notion of resolution function was used in Ref. [36]. We first describe the method in some generality. It is a completely model-independent approach since no *ansatz* needs to be made for the spectral function.

The goal is to solve the integral equation

$$G(x_i) = \int_0^\infty d\omega f(\omega) K(x_i,\omega), \qquad x_i \neq 0 \quad \forall\ i \tag{34}$$

for the unknown function $f(\omega)$, given the kernel $K(x_i,\omega)$ and given data on $G(x_i)$. The idea is to define an estimator $\hat{f}(\bar{\omega})$

$$\hat{f}(\bar{\omega}) = \int_0^\infty \hat{\delta}(\bar{\omega},\omega) f(\omega) d\omega \tag{35}$$

where $\hat{\delta}(\bar{\omega},\omega)$ is called the resolution function or averaging kernel. It is a smooth function concentrated around some reference value $\bar{\omega}$, normalized according to $\int_0^\infty d\omega \hat{\delta}(\bar{\omega},\omega) = 1$, and parametrized at fixed $\bar{\omega}$ by coefficients $q_i(\bar{\omega})$,

$$\hat{\delta}(\bar{\omega},\omega) = \sum_i q_i(\bar{\omega}) K_i(\omega), \tag{36}$$

so that $\hat{f}$ is obtained according to

$$\hat{f}(\bar{\omega}) = \sum_{i=1}^{n} G(x_i) q_i(\bar{\omega}). \tag{37}$$

The goal is then to minimize the width of the resolution function. Minimizing the second moment of $\hat{\delta}(\bar{\omega},\omega)^2$ in its second argument around its first argument yields

$$q_i(\bar{\omega}) = \frac{\sum_j W_{ij}^{-1}(\bar{\omega}) R(x_j)}{\sum_{k,l} R(t_k) W_{kl}^{-1}(\bar{\omega}) R(x_l)}, \tag{38}$$

where

$$W_{ij}(\bar{\omega}) = \int_0^\infty d\omega K(x_i,\omega)(\omega-\bar{\omega})^2 K(x_j,\omega), \tag{39}$$

$$R(x_i) = \int_0^\infty K(x_i,\omega) d\omega. \tag{40}$$

We remark that $\hat{f}(\omega)$ equals $f(\omega)$ if the latter is constant.

The matrix $W_{ij}(\bar{\omega})$ is very close to being singular. This is the reason why, when trying to use a data set with error bars, one needs to regulate the inverse problem, replacing the matrix W by

$$W_{ij} \to \lambda W_{ij} + (1-\lambda) S_{ij}, \qquad 0 < \lambda < 1, \tag{41}$$

where S_{ij} is the covariance matrix of the data. The value of λ controls the trade-off between resolution and stability. For values of λ close to 1, we obtain the best possible resolution. However the results tend to be unstable since the matrix is poorly conditioned and large cancellations take place among the terms in Eq. (37). Reducing λ improves the stability of the result at the cost of deteriorating the frequency resolution. One may start from a value for λ near unity and decrease it until the statistical error on $\hat{\rho}(\omega)$ drops to say 5%. Of all linear methods, the result $\hat{\rho}(\omega)$ then has the best possible frequency resolution [as measured by the second moment of $\delta(\bar{\omega},\omega)^2$ in its second argument] for the given statistical uncertainty of 5%. It should be emphasized that, as a matter of principle, any choice of λ yields a correct result, in the sense that the relation between $\hat{\rho}(\omega)$ and $\rho(\omega)$ is given model independently by the resolution function. However, in order to be useful, the result must have both a reasonable statistical uncertainty and a decent frequency resolution. It is worth noting that if the statistical accuracy of the input correlator is increased by a factor ξ (so that S_{ij} is overall reduced by a factor $1/\xi$), then keeping λ constant will result in a better frequency resolution; instead, choosing a new value for λ so as to keep $(1-\lambda)S_{ij}$ constant will maintain the same resolution function and $\hat{\rho}(\omega)$ will have a reduced statistical uncertainty by $1/\sqrt{\xi}$. In particular, it is predictable by how much the statistics needs to be increased in order to achieve a certain frequency resolution at fixed statistical uncertainty.

We apply this method to Eq. (14). In order to regularize the finite-temperature kernel at $\omega = 0$ we rewrite the equation as

$$G_A(x_0,T,\mathbf{p}) = \int_0^\infty d\omega \left(\frac{\rho^A(\omega,\mathbf{p})}{\tanh(\omega/2)}\right) \underbrace{\left(\frac{\cosh(\omega(\beta/2-x_0))}{\cosh(\omega\beta/2)}\right)}_{\doteq K(x_0,\omega)}. \tag{42}$$

This defines our estimator $\hat{\rho}$ at $\omega = \bar{\omega}$,

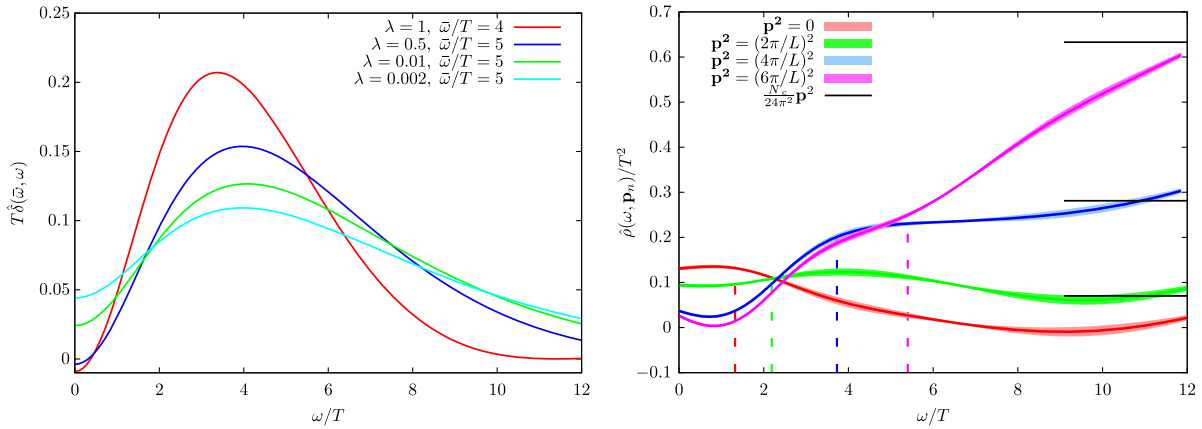

FIG. 7 (color online). Left: Some examples of resolution functions for different values of λ centered at $\bar{\omega}/T$. Right: Estimators $\hat{\rho}(\omega,\mathbf{p}_n)/T^2$ for $n = 0, 1, 2, 3$ together with its error shown as a band. The vertical colored dashed lines correspond to the locations of the expected positions of the poles $\omega_{\mathbf{p}_n}$ according to Eq. (11) with $u(T) = u_m$. The black horizontal lines correspond to the tree-level asymptotic values of $\rho^A(\omega,\mathbf{p})$. All renormalization constants have been taken into account as well as the improvement program on the axial correlators. Dimensionful quantities have been made dimensionless by the appropriate power of $T = 1/24a$.

$$\hat{\rho}(\bar{\omega},\mathbf{p}) = \int_0^\infty d\omega\hat{\delta}(\bar{\omega},\omega)\left(\frac{\rho_A(\omega,\mathbf{p})}{\tanh(\omega\beta/2)}\right). \qquad (43)$$

After regulating the problem via the covariance matrix S_{ij} as in Eq. (41), the inversion is carried out via singular value decomposition. This offers the opportunity to diagnose how badly conditioned the matrix is. With all quantities made dimensionless by applying appropriate powers of the temperature, we choose $\lambda = 2\cdot 10^{-3}$ in the following, so as to yield an error $\lesssim 5\%$ on $\hat{\rho}$. Typical condition numbers of the regularized matrix in Eq. (41) are $\sim 10^8$. The situation gets worse when λ approaches unity, as explained above. The results for zero momentum and the first three units of momentum are shown in the right panel of Fig. 7. As in the case of the fit, we included the points of the correlation in the interval $x_0/a = [5, 12]$ so $W_{ij}(\bar{\omega})$ is an $n\times n$ symmetric matrix with $n = 8$. With our chosen value of λ, we obtain a relative error on $\hat{\rho}$ of $\sim$3–5%, while the resolution function is displayed in the left panel of Fig. 7. One direct observation is the fact that the expected asymptotic behavior for large values of ω is reproduced very well.

The right panel of Fig. 7 also shows the expected positions of the poles that follow from Eq. (11) as vertical colored dashed lines. We now want to test the $\mathbf{p}$ dependence of the residue $\mathrm{Res}(\omega_{\mathbf{p}})$ via the following argument. If we assume that, for a given value of ω, $\hat{\rho}(\omega,\mathbf{p})$ is dominated by the pion pole, we obtain the following estimator for the residue:

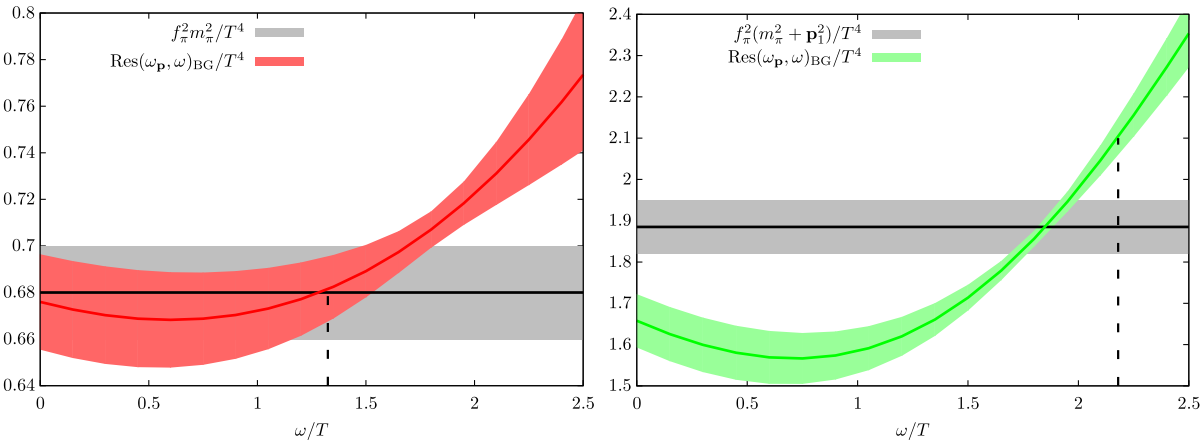

FIG. 8 (color online). The effective residue $\mathrm{Res}(\omega_{\mathbf{p}},\omega)_{\mathrm{BG}}$ as defined in Eq. (44). Left: No momentum induced, $\mathbf{p} = 0$. Right: One unit of momentum induced, $\mathbf{p}_1 = (0, 0, 2\pi/L)$. The grey band is the expectation in terms of screening quantities [Eq. (20)]. All renormalization factors are included. The errors arise from the statistical uncertainty. The values of $\omega_{\mathbf{p}}$ are indicated by dashed vertical lines.

$$\mathrm{Res}(\omega_{\mathbf{p}},\omega)_{\mathrm{BG}} = \frac{2\omega_{\mathbf{p}}\tanh(\omega_{\mathbf{p}}\beta/2)\hat{\rho}(\omega,\mathbf{p})}{\hat{\delta}(\omega,\omega_{\mathbf{p}})}. \quad (44)$$

Here we treat $\omega_{\mathbf{p}}$ as input and calculate it using Eq. (11) with the value of $u = u_m = 0.74(1)$ determined at zero momentum. The result as a function of ω is shown in Fig. 8 for zero and one unit of momentum. The natural choice where $\mathrm{Res}(\omega_{\mathbf{p}},\omega)_{\mathrm{BG}}$ is expected to be the best estimator of the residue is at $\omega \approx \omega_{\mathbf{p}}$. Looking at Fig. 8, one sees that approximately around this value the curve intercepts the grey band, which represents the prediction (20). The latter is particularly well verified at zero momentum, while the agreement at $|\mathbf{p}| = |\mathbf{p}_1| \approx 400$ MeV is at the ten percent level. These observations provide a further test that the pion dispersion relation (11) predicted by the thermal chiral effective theory is consistent with the lattice two-point function of the axial-charge density.

Comparing the method followed in this subsection with the previous method based on a global fit to the spectral function, the former has the advantage of not requiring an explicit parametrization of the non-pion contributions to the spectral function. This observation may be useful in other lattice studies of spectral functions.

V. CONCLUSION

We have found that the pion quasiparticle mass is reduced significantly by thermal effects compared to its vacuum value—unlike the pion screening mass, which increases. Also, the energy cost of giving the pion quasiparticle a momentum is significantly reduced, since the "velocity" is well below unity, $u \approx 0.74$. We have tested that the pion indeed admits a modified dispersion relation, Eq. (11), by analyzing lattice two-point functions. The test is based on requiring the consistency with the lattice data of the combined chiral prediction for the dispersion relation and the residue of the pion pole in the two-point function of the axial-charge density. These conclusions could be strengthened further by repeating the calculation at smaller quark masses and with higher statistics. Discretization errors should also be studied. Having a higher resolution in momentum could help in assessing the region of validity of the chiral effective theory.

Assuming the results hold to further scrutiny, one may wonder how much a modified mass and dispersion relation of the pion affects (a) the freeze-out mechanism in heavy-ion collisions and (b) the predictions of the hadron resonance gas model for equilibrium properties. In answering the latter question, one must take into account that the modification of the pion dispersion relation is due to the presence of hadrons in the medium, and issues of double counting arise. However, the following estimates may provide a useful first idea of the size of the effect. At the temperature of 169 MeV in the two-flavor theory that we have been discussing, with a zero-temperature pion mass of 270 MeV, we estimate, using the hadron resonance gas model, an isovector quark number susceptibility[5] amounting to $\chi_s/T^2 = 0.42$. In the HRG model, the pion contributes[6] $\chi_s/T^2|_{\mathrm{pions}} = 4\beta^3 \int \frac{d^3p}{(2\pi)^3} f_B(p)(1+f_B(p)) = 0.28$. If the spatial-momentum integral in the pion contribution is cut off at $p_{\max} = 400$ MeV (roughly the range of validity of the chiral effective theory that we found), the contribution is reduced to 0.11. If we instead use the modified dispersion relation with the lower quasiparticle mass $\omega_{\mathbf{0}} = 223$ MeV and $u = 0.74$, the contribution for $p < p_{\max}$ amounts again to 0.28. It is unclear whether one should include a contribution from higher momenta, given that the thermal width of the pion may then not be negligible. The numbers above illustrate that the contribution of the pion to the quark number susceptibility might not be as strongly affected as one may at first think. However, the contribution comes from softer pions, which implies a reduced amplitude of the transport peak in the two-point function of the vector current $V_i^a(x)$, an effect that can be tested in lattice simulations.

Determining the dispersion relation of a non-Goldstone hadron would be interesting to see whether the relatively strong change we have seen in the pion properties is specific to chiral dynamics. In general, a kinetic theory description allows one to use as primary degrees of freedom the quasiparticles specific to the temperature of interest. It is therefore much broader in applicability than the hadron resonance gas model, but requires input information on the quasiparticles. The channel treated here illustrates the importance of having guidance from an effective theory in reconstructing the gross features of the spectral function. In doing so, applying the Backus-Gilbert method in a first step can be useful in narrowing down the region of frequency where a specific *ansatz* for the spectral function must be made.

ACKNOWLEDGMENTS

We are grateful for the access to the zero-temperature ensemble used here, made available to us through CLS, and for the zero-temperature correlation functions generated within the Mainz lattice group. We acknowledge the use of computing time for the generation of the gauge configurations on the *JUGENE* and *JUQUEEN* computers of the Gauss Centre for Supercomputing located at Forschungszentrum Jülich, Germany, allocated through the John von Neumann Institute for Computing (NIC) within project HMZ21. Part of the configurations and all correlation functions were computed on the dedicated QCD platforms "*Wilson*" at the Institute for Nuclear Physics, University of Mainz, and "*Clover*" at the Helmholtz-Institut Mainz. This work was supported by the Center for Computational Sciences in Mainz as part of the Rhineland-Palatinate Research Initiative and by the DFG

[5]The current is here normalized as $\sqrt{2}V_\mu^a(x)$; see Eq. (1).
[6]Here $f_B(p) = (e^{\beta\omega_p} - 1)^{-1}$ is the Bose distribution.

Grant No. ME 3622/2-1 *Static and dynamic properties of QCD at finite temperature*. During part of this research A. F. was supported by the Natural Sciences and Engineering Research Council of Canada (NSERC).

APPENDIX A: TENSOR STRUCTURE OF THE AXIAL CURRENT TWO-POINT FUNCTIONS

We work in the Euclidean field theory and define the correlation function in momentum space as

$$\delta^{ab}\Pi^{\mathrm{A}}_{\mu\nu}(\hat{\epsilon},k) \equiv \int d^4x e^{ik\cdot x}\langle A^a_\mu(x)A^b_\nu(0)\rangle_{\hat{\epsilon}}. \tag{A1}$$

The unit vector $\hat{\epsilon}$ points in the direction that defines the thermal boundary condition. It is $\hat{\epsilon}=(1,0,0,0)$ in the rest frame of the thermal system. By doing the change of integration variables $x\to -x$ and using translation invariance

$$\langle A_\mu(-x)A_\nu(0)\rangle_{\hat{\epsilon}} = \langle A_\nu(x)A_\mu(0)\rangle_{\hat{\epsilon}} \tag{A2}$$

and symmetry under the O(4) rotation $x\to -x$,

$$\langle A_\mu(-x)A_\nu(0)\rangle_{\hat{\epsilon}} = \langle A_\mu(x)A_\nu(0)\rangle_{-\hat{\epsilon}}, \tag{A3}$$

we have the symmetries

$$\Pi^{\mathrm{A}}_{\mu\nu}(\hat{\epsilon},k) = \Pi^{\mathrm{A}}_{\nu\mu}(\hat{\epsilon},-k) = \Pi^{\mathrm{A}}_{\mu\nu}(-\hat{\epsilon},-k). \tag{A4}$$

To write down the tensor decomposition, we have the building blocks $\delta_{\mu\nu}$, k_μ and $\hat{\epsilon}_\mu$ at our disposal. We can write down four structures that respect the symmetries (A4),

$$\delta_{\mu\nu}, \qquad \frac{k_\mu k_\nu}{k^2}, \qquad \frac{\hat{\epsilon}\cdot k}{k^2}(\hat{\epsilon}_\mu k_\nu + k_\mu\hat{\epsilon}_\nu), \qquad \hat{\epsilon}_\mu\hat{\epsilon}_\nu. \tag{A5}$$

We can form one projector to the subspace orthogonal to both $\hat{\epsilon}$ and k,

$$C^{\mathrm{T,t}}_{\mu\nu} = \delta_{\mu\nu} - \frac{1}{1-(\hat{\epsilon}\cdot k)^2/k^2}\left(\hat{\epsilon}_\mu\hat{\epsilon}_\nu + \frac{k_\mu k_\nu}{k^2} - \frac{1}{k^2}(\hat{\epsilon}\cdot k)(\hat{\epsilon}_\mu k_\nu + k_\mu\hat{\epsilon}_\nu)\right), \tag{A6}$$

and one projector onto the component of $\hat{\epsilon}$ which is orthogonal to k,

$$C^{\mathrm{T,l}}_{\mu\nu} = \delta_{\mu\nu} - \frac{k_\mu k_\nu}{k^2} - C^{\mathrm{T,t}}_{\mu\nu} = \frac{1}{1-(\hat{\epsilon}\cdot k)^2/k^2}\left(\hat{\epsilon}_\mu - \frac{(\hat{\epsilon}\cdot k)k_\mu}{k^2}\right)\left(\hat{\epsilon}_\nu - \frac{(\hat{\epsilon}\cdot k)k_\nu}{k^2}\right). \tag{A7}$$

Two possible nontransverse combinations are

$$C^{\mathrm{L,l}}_{\mu\nu} = \frac{k_\mu k_\nu}{k^2}, \qquad C^{\mathrm{M}}_{\mu\nu} = \frac{1}{1-(\hat{\epsilon}\cdot k)^2/k^2}\left(\hat{\epsilon}_\mu\hat{\epsilon}_\nu - (\hat{\epsilon}\cdot k)^2\frac{k_\mu k_\nu}{(k^2)^2}\right). \tag{A8}$$

The first one is the projector onto the direction of k_μ. The second tensor, while not a projector, has the properties

$$C^{\mathrm{M}}_{\mu\mu} = 1, \qquad C^{\mathrm{T,t}}_{\mu\alpha}C^{\mathrm{M}}_{\alpha\nu} = C^{\mathrm{L,l}}_{\mu\alpha}C^{\mathrm{M}}_{\alpha\nu} = 0. \tag{A9}$$

In summary, we can write

$$\Pi^{\mathrm{A}}_{\mu\nu}(\hat{\epsilon},k) = C^{\mathrm{T,t}}_{\mu\nu}\Pi^{\mathrm{T,t}} + C^{\mathrm{T,l}}_{\mu\nu}\Pi^{\mathrm{T,l}} + C^{\mathrm{L,l}}_{\mu\nu}\Pi^{\mathrm{L,l}} + C^{\mathrm{M}}_{\mu\nu}\Pi^{\mathrm{M}}. \tag{A10}$$

The argument of the C's is $(\hat{\epsilon},k)$, while the argument of the form factors Π is $(\hat{\epsilon}\cdot k,k^2)$.

It is helpful to be able to invert the relation (A10) in order to project out the form factors individually. We find

$$\Pi^{\mathrm{L,l}} = \frac{k_\mu k_\nu}{k^2}\Pi^A_{\mu\nu}, \tag{A11}$$

$$\Pi^{\mathrm{M}} = \frac{1}{\hat{\epsilon}\cdot k}k_\mu\Pi^A_{\mu\nu}\left(\hat{\epsilon}_\nu - \frac{\hat{\epsilon}\cdot k}{k^2}k_\nu\right), \tag{A12}$$

$$\Pi^{\mathrm{T,l}} = \frac{1}{1-(\hat{\epsilon}\cdot k)^2/k^2}\left[\hat{\epsilon}_\mu\Pi^A_{\mu\nu}\hat{\epsilon}_\nu - \frac{(\hat{\epsilon}\cdot k)^2}{(k^2)}\Pi^{\mathrm{L,l}} - (1+(\hat{\epsilon}\cdot k)^2/k^2)\Pi^{\mathrm{M}}\right], \tag{A13}$$

$$\Pi^{\mathrm{T,t}} = \frac{1}{2}\{\Pi^A_{\mu\mu} - [\Pi^{\mathrm{T,l}} + \Pi^{\mathrm{M}} + \Pi^{\mathrm{L,l}}]\}. \tag{A14}$$

1. Special kinematics

When $(\hat{\epsilon}\cdot k)^2 = k^2$, corresponding to vanishing spatial momentum in the rest frame of the thermal system, the projectors $C^{\mathrm{T,t}}_{\mu\nu}$ and $C^{\mathrm{T,l}}_{\mu\nu}$ as well as $C^{\mathrm{M}}_{\mu\nu}$ become singular. Therefore we will define the value of the form factors in this

limit by continuity. When $\hat{\epsilon}$ and k are collinear, there are only two independent tensor structures,

$$\Pi^{A,\mathrm{col}}_{\mu\nu}(\hat{\epsilon},k)=\left(\delta_{\mu\nu}-\frac{k_\mu k_\nu}{k^2}\right)\hat{\Pi}_{\mathrm{T}}(k^2)+\frac{k_\mu k_\nu}{k^2}\hat{\Pi}_{\mathrm{L}}(k^2). \quad \text{(A15)}$$

Applying the relevant projectors as in Eqs. (A11)–(A14), one finds that

$$\Pi^{\mathrm{T,t}}=\Pi^{\mathrm{T,l}}=\hat{\Pi}_{\mathrm{T}},\qquad \Pi^{\mathrm{L,l}}=\hat{\Pi}_{\mathrm{L}},\qquad \Pi^{\mathrm{M}}=0. \quad \text{(A16)}$$

When $\hat{\epsilon}\cdot k=0$, corresponding to the static correlators, $C^{\mathrm{T,l}}_{\mu\nu}$ becomes equal to $C^{\mathrm{M}}_{\mu\nu}$. Therefore, in that situation the Euclidean correlator is only sensitive to the sum of the two corresponding form factors, $(\Pi^{\mathrm{M}}+\Pi^{T,l})$. Equation (A12) nonetheless provides an unambiguous definition of Π^{M} if, expressed in the rest frame, $\lim_{k_0\to 0}\Pi^{A}_{0i}/k_0$ is known. The latter limit, however, requires an analytic continuation of the Euclidean correlator.

2. The zero-temperature limit

At zero temperature, it is natural to parametrize the correlation function as

$$\Pi^{\mathrm{A}}_{\mu\nu}(k)=\left(\delta_{\mu\nu}-\frac{k_\mu k_\nu}{k^2}\right)\Pi^{\mathrm{T}}(k^2)+\frac{k_\mu k_\nu}{k^2}\Pi^{\mathrm{L}}(k^2). \quad \text{(A17)}$$

Applying the same projectors as in Eqs. (A11)–(A14) onto the correlation function (A17), and requiring that the same result be obtained in the zero-temperature limit, we obtain

$$\Pi^{\mathrm{L,l}}(\hat{\epsilon}\cdot k,k^2)\to\Pi^{\mathrm{L}}(k^2), \quad \text{(A18)}$$

$$\Pi^{\mathrm{M}}(\hat{\epsilon}\cdot k,k^2)\to 0, \quad \text{(A19)}$$

$$\Pi^{\mathrm{T,l}}(\hat{\epsilon}\cdot k,k^2)\to\Pi^{\mathrm{T}}(k^2), \quad \text{(A20)}$$

$$\Pi^{\mathrm{T,t}}(\hat{\epsilon}\cdot k,k^2)\to\Pi^{\mathrm{T}}(k^2). \quad \text{(A21)}$$

3. Relation to the correlators of the pseudoscalar density

We define

$$\delta^{ab}\mathcal{A}_\mu(\hat{\epsilon},k)=\int d^4x e^{ikx}\langle A^a_\mu(x)P^b(0)\rangle, \quad \text{(A22)}$$

$$\delta^{ab}\mathcal{P}(\hat{\epsilon},k)=\int d^4x e^{ikx}\langle P^a(x)P^b(0)\rangle. \quad \text{(A23)}$$

We note the symmetry relations

$$\mathcal{A}_\mu(\hat{\epsilon},k)=-\mathcal{A}_\mu(-\hat{\epsilon},-k), \quad \text{(A24)}$$

$$\int d^4x e^{ikx}\langle P(x)A_\nu(0)\rangle_{\hat{\epsilon}}=\mathcal{A}_\nu(\hat{\epsilon},-k), \quad \text{(A25)}$$

respectively from O(4) invariance and from translation invariance.

In Ref. [8] (see Eqs. (A7) and (A8) in that reference), taking into account Eqs. (A25) and (A4), the Ward identities

$$2m\mathcal{A}_\mu(\hat{\epsilon},k)=ik_\alpha\Pi^{\mathrm{A}}_{\mu\alpha}(\hat{\epsilon},k), \quad \text{(A26)}$$

$$4m^2\mathcal{P}(\hat{\epsilon},k)=k_\mu\Pi^{\mathrm{A}}_{\mu\alpha}(\hat{\epsilon},k)k_\alpha+m\langle\bar{\psi}\psi\rangle \quad \text{(A27)}$$

were derived. Inserting our tensor decomposition of $\Pi^{\mathrm{A}}_{\mu\alpha}(\hat{\epsilon},k)$, we find

$$2m\mathcal{A}_\mu(\hat{\epsilon},k)=ik_\mu\Pi^{\mathrm{L,l}}(\hat{\epsilon}\cdot k,k^2)+i(\hat{\epsilon}\cdot k)\frac{\hat{\epsilon}_\mu-(\hat{\epsilon}\cdot k/k^2)k_\mu}{1-(\hat{\epsilon}\cdot k)^2/k^2}\Pi^{\mathrm{M}}(\hat{\epsilon}\cdot k,k^2), \quad \text{(A28)}$$

$$4m^2\mathcal{P}(\hat{\epsilon},k)=k^2\Pi^{\mathrm{L,l}}(\hat{\epsilon}\cdot k,k^2)+m\langle\bar{\psi}\psi\rangle. \quad \text{(A29)}$$

APPENDIX B: ON THE RESIDUE OF THE PION POLE

In this appendix, we use the general results of the previous section in the rest frame of the thermal system, $\hat{\epsilon}_\mu=(1,0,0,0)$. The form factors are thus functions of k_0 and k^2 and the dependence on $\hat{\epsilon}$ is no longer indicated explicitly. All expressions for correlation functions in this section refer exclusively to the pion contribution.

In Ref. [8], it was shown that the residue of the pion pole in the two-point function of A_0 at vanishing spatial momentum is $\mathrm{Res}(\omega_{\mathbf{0}})=f_\pi^2m_\pi^2$. In order to determine the form of the residue at finite momentum, we parametrize the residue as

$$\mathrm{Res}(\omega_{\mathbf{k}})=f_\pi^2(m_\pi^2+\lambda\mathbf{k}^2). \quad \text{(B1)}$$

To determine the parameter λ, we will exploit the fact that the spectral representation of the two-point function of A_0 in terms of real-time excitations must agree with the spectral representation in terms of screening states. From the former point of view, the pion contribution to the correlator in momentum space takes the form

$$\Pi^{A}_{00}(k)=\frac{f_\pi^2(m_\pi^2+\lambda\mathbf{k}^2)}{k_0^2+\omega_{\mathbf{k}}^2}, \quad \text{(B2)}$$

with $\omega_{\mathbf{k}}$ given in Eq. (11). From the "screening" point of view, the residue must be proportional to k_0^2 at small k_0^2 (here we invoke the analytic continuation in the frequency, away from the Matsubara values $k_0=2\pi Tn$). This is so

because the screening pion is odd under the Euclidean time reversal $x_0 \to -x_0$, while A_0 is even. Thus we can write

$$\Pi^A_{00}(k) = \frac{-|F|^2 k_0^2}{\mathbf{k}^2 + \frac{k_0^2}{u^2} + m_\pi^2} \tag{B3}$$

for some parameter F to be determined. Equations (B2) and (B3) must agree when the numerators are evaluated at the pole, $k_0^2 = -\omega_{\mathbf{k}}^2$. From here we learn the following:

$$|F| = \frac{f_\pi}{u^2}, \qquad \lambda = 1. \tag{B4}$$

This shows in particular that the residue has the form given in Eq. (20). Essentially the same argument was already used in Ref. [8] to determine the residue of the pion pole in the two-point function of the pseudoscalar density,

$$\mathcal{P}(k) = -\frac{\langle\bar\psi\psi\rangle^2 u^2}{4f_\pi^2}\frac{1}{k_0^2 + \omega_{\mathbf{k}}^2}. \tag{B5}$$

We note that for a one-pole contribution, factorization relations such as

$$|\mathcal{A}_0(k)|^2 = |\mathcal{P}(k)||\Pi^A_{00}(k)| \tag{B6}$$

hold. The phase of $\mathcal{A}_0$ can then be determined through its form at vanishing spatial momentum given in Ref. [8].

1. The pion contribution to $\Pi^A_{\mu\nu}$

Having found the residue of the pion pole in the various two-point functions of the axial current, we give for completeness the pion contribution to the form factors defined in Eqs. (A11)–(A14),

$$\Pi^{\mathrm{L,l}}(k_0, k^2) = -\frac{f_\pi^2 m_\pi^4 u^2}{k^2(k_0^2 + \omega_{\mathbf{k}}^2)}, \tag{B7}$$

$$\Pi^{\mathrm{M}}(k_0, k^2) = \frac{f_\pi^2 m_\pi^2 \mathbf{k}^2(1-u^2)}{k^2(k_0^2 + \omega_{\mathbf{k}}^2)}, \tag{B8}$$

$$\Pi^{\mathrm{T,l}}(k_0, k^2) = \frac{f_\pi^2 \mathbf{k}^2(1-u^2)}{k_0^2 + \omega_{\mathbf{k}}^2}, \tag{B9}$$

$$\Pi^{\mathrm{T,t}}(k_0, k^2) = 0. \tag{B10}$$

The first is obtained from Eq. (A29), then the second from Eq. (A28), and the third by using Eq. (A13) and the first two results. Via Eq. (A10), the form factors allow one to obtain the entire tensor $\Pi^A_{\mu\nu}$.

These calculations could be greatly expedited by using an effective Lagrangian, as written down in Ref. [11]. However it is also instructive to derive the results above directly within QCD.

APPENDIX C: MOCK-DATA STUDY OF THE BACKUS-GILBERT METHOD

In this appendix, we study the performance of the Backus-Gilbert method in a realistic lattice QCD application. We apply the method on mock data, where the underlying spectral function is known. Our goal is to validate the method used in Sec. IV E.

Our procedure is the following:

(1) We start from a real lattice correlator computed on the "zero"-temperature ensemble O7 introduced in Sec. III and Table I.
(2) In order to construct a realistic model, a spectral function with sufficiently many free parameters is fitted to the lattice data.
(3) The original correlator data is now replaced by mock data, namely the correlator obtained by integrating the fitted spectral function, with Gaussian noise added (using the original covariance matrix of the correlator).
(4) The mock data is now fed into the Backus-Gilbert method, which generates a filtered spectral function $\hat\rho_{\mathrm{BG}}(\bar\omega)$ and the resolution function $\delta(\bar\omega, \omega)$. The former is compared to the input spectral function.
(5) The final step, as in Sec. IV E, is to assume that the true spectral function is dominated at low frequencies by the contribution of a stable particle (the pion), and we determine its residue in the correlator from $\hat\rho_{\mathrm{BG}}(\omega)$ and $\delta(\bar\omega, \omega)$. The result is compared with the input value.

1. Construction of realistic mock data

We use the Euclidean pseudoscalar density correlator projected onto zero momentum due to its good signal-to-noise ratio,

$$G_P(x_0)\delta^{ab} = -\int d^3x \langle P^a(x) P^b(0)\rangle. \tag{C1}$$

In a first step, we want to obtain a fit function $G_P^{\mathrm{fit}}(x_0)$ which describes the data. We employ the following fit *ansatz* for the spectral function:

$$\rho_P(\omega) = \frac{A_1}{2} e^{\omega_0\beta/2}\delta(\omega - \omega_0) + \frac{A_2 N_c}{(4\pi)^2}\theta(\omega - 3\omega_0)\omega^2. \tag{C2}$$

It contains a δ-type pion contribution at a low frequency ω_0 and a continuum of multiparticle states beginning at threshold $\omega = 3\omega_0$ due to the negative parity of the pseudoscalar density operator. The corresponding correlator is given by[7]

[7]The integrand in Eq. (C3) should really be divided by $(1 + \exp(-\beta\omega))$, but we neglect this effect because $\omega_0\beta \simeq 8.8$.

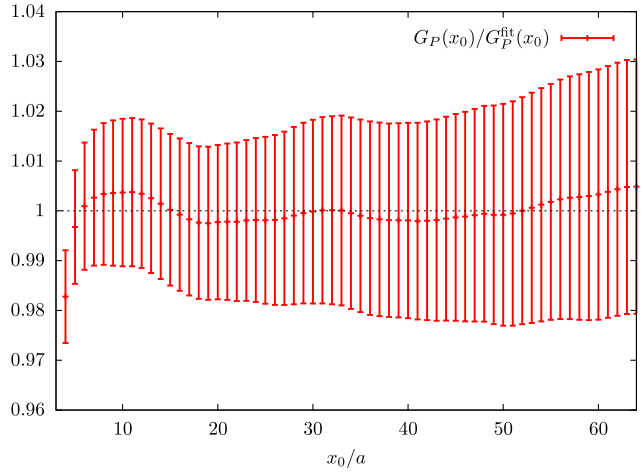

FIG. 9 (color online). Euclidean correlator $G_P(x_0)$ divided by its fit function $G_P^{\rm fit}(x_0)$.

$$G_P^{\rm fit}(x_0) = \int_0^\infty d\omega \rho_P(\omega)(e^{-\omega x_0} + e^{-\omega(\beta - x_0)}) \quad \text{(C3)}$$

$$= A_1 \cosh(\omega_0(\beta/2 - x_0)) + \frac{A_2 N_c}{(4\pi)^2}\left[\frac{e^{-3\omega_0 x_0}}{x_0^3}(2 + 6\omega_0 x_0 + 9\omega_0^2 x_0^2) + (x_0 \to \beta - x_0)\right]. \quad \text{(C4)}$$

The fit to the data was performed in the interval $x_0/a \in [5, 64]$ in order to avoid cutoff effects present at small distances. In view of Fig. 9 one clearly sees that $G_P^{\rm fit}(x_0)$ describes the data in a satisfactory way yielding an (uncorrelated) $\chi^2/\text{d.o.f.} \sim 10^{-2}$ with fit parameters shown in Table V. Note that we do not quote statistical errors on the parameters A_1, ω_0 and A_2 since our goal is merely to construct realistic mock data.

The next step is to generate the correlator $G_P^{\rm fit}(x_0)$ that corresponds to the fitted spectral function via the integral transform (C3). In order to be as realistic as possible, we add Gaussian noise $\delta G_P^{\rm fit}(x_0)$ to the correlator in order to obtain the mock data $\tilde{G}_P^{\rm fit}$,

$$\tilde{G}_P^{\rm fit}(x_0) = G_P^{\rm fit}(x_0) + \delta G_P^{\rm fit}(x_0). \quad \text{(C5)}$$

The noise is generated by using the covariance matrix S_{ij} of the real data $G_P(x_0^i)$ where i and j label the discrete lattice points. The eigenvalues and eigenvectors of S are obtained by solving the eigenvalue equation

$$Sv^{(i)} = (\sigma^2)^{(i)} v^{(i)}. \quad \text{(C6)}$$

The statistically independent observables $U^{(i)}$ with squared variance $(\sigma^2)^{(i)}$ are linear combinations of the points $G_P(x_0^i)$,

$$U^{(i)} = (V^T)_{ij} G_P(x_0^j), \quad \text{(C7)}$$

where the orthogonal matrix V carries the eigenvectors written in columns and diagonalizes S via $V^T S V = D$. Random values $\delta U^{(i)}$ are generated according to the normalized Gaussian probability distribution

$$P(\delta U^{(i)}) = \frac{1}{\sqrt{2\pi(\sigma^2)^{(i)}}} e^{-\frac{(\delta U^{(i)})^2}{2(\sigma^2)^{(i)}}} \quad \text{(C8)}$$

and by back-substitution we obtain the random noise

$$\delta G_P^{\rm fit}(x_0^i) = (V)_{ij} \delta U^{(j)}. \quad \text{(C9)}$$

TABLE V. Fit parameters corresponding to $G_P^{\rm fit}(x_0)$. Dimensionful quantities are made dimensionless by dividing with $T = 1/128a$. No renormalization constants are included.

A_1/T^3	463.911
ω_0/T	8.394
A_2	5.727

2. The Backus-Gilbert method applied to $\tilde{G}_P^{\rm fit}(x_0)$

We now use the Backus-Gilbert algorithm on the mock-data $\tilde{G}_P^{\rm fit}(x_0)$ with the goal to "reproduce" the spectral function $\rho_P(\omega)$ with parameters in Table V. We write the following identity based on Eq. (C3)

$$\tilde{G}_P^{\rm fit}(x_0) = \int_0^\infty d\omega \left(\frac{\rho_P(\omega)}{\omega^2}\right) \underbrace{\omega^2(e^{-\omega x_0} + e^{-\omega(\beta - x_0)})}_{\doteq K(x_0,\omega)} \quad \text{(C10)}$$

so that the output $\hat{\rho}_{\rm BG}(\omega)$ of the Backus-Gilbert method is a "filtered" version of $\frac{\rho_P(\omega)}{\omega^2}$,

$$\hat{\rho}_{\rm BG}(\bar{\omega}) = \int_0^\infty d\omega \hat{\delta}(\bar{\omega}, \omega)\left(\frac{\rho_P(\omega)}{\omega^2}\right). \quad \text{(C11)}$$

The results are shown in the left panel of Fig. 10, which corresponds to a value of the regulating parameter $\lambda = 0.25$, and the points considered in the Backus-Gilbert method belong to the interval $x_0^i/a \in [5, 20]$. Consequently, the dimension of all matrices and vectors defined previously is $M = 16$. In view of Fig. 10 one sees that the location of the pion pole agrees with the value quoted in Table V. The same is true for the height of the threshold, whose expectation is $\frac{A_2 N_c}{(4\pi)^2}$ and its flatness is consistent with the assumed ω^2 growth of $\rho_P(\omega)$.

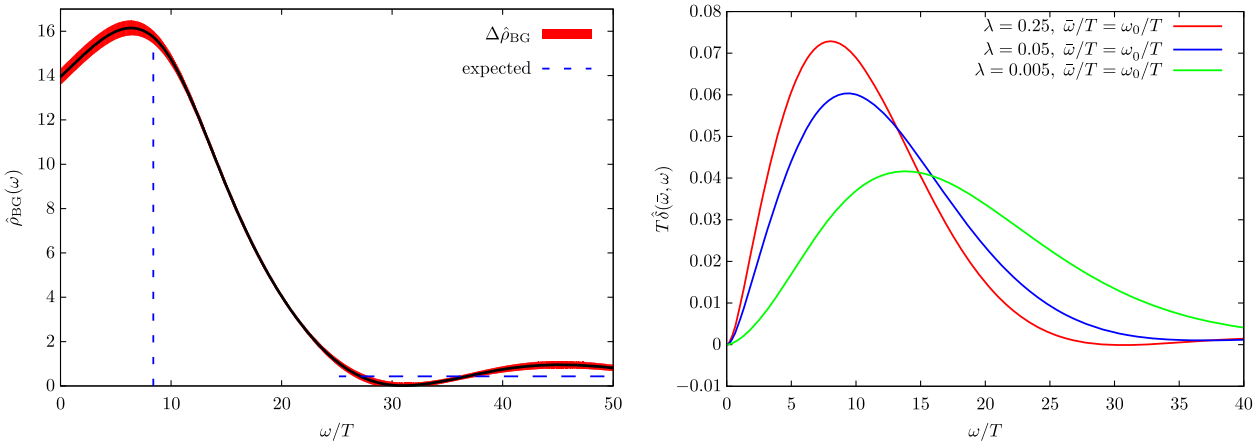

FIG. 10 (color online). Left: Estimator $\hat{\rho}_{\rm BG}(\omega)$ with $\lambda = 0.25$. Expected values are shown as dashed blue lines. Right: Resolution functions $\hat{\delta}(\omega_0,\omega)$ for different values of λ.

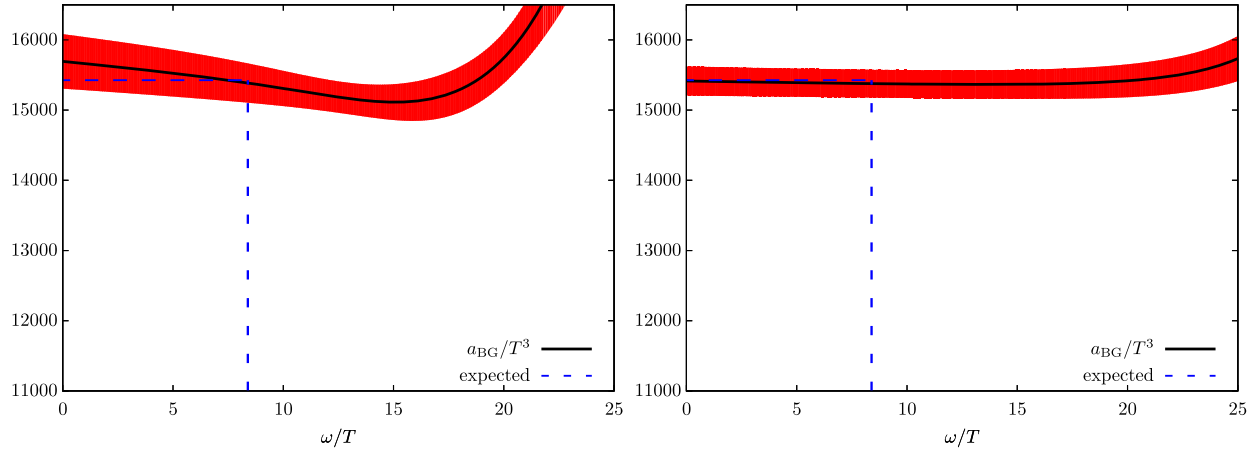

FIG. 11 (color online). The estimator $a_{\rm BG}/T^3$ as defined in Eq. (C12) with $T = 1/128a$ as a function of ω Left: $\lambda = 0.25$. Right: $\lambda = 0.005$.

3. Extraction of the pion residue

We now extract the residue of the pion in the correlator from the output of the Backus-Gilbert method. As in Eq. (44), we assume that at small frequencies $\hat{\rho}$ is dominated by the pion and therefore $\rho_P(\omega) = a_{\rm BG}\delta(\omega-\omega_0)+\cdots$. Using Eq. (C11), we define an estimator $a_{\rm BG}(\omega)$,

$$a_{\rm BG}(\omega) = \frac{\hat{\rho}_{\rm BG}(\omega)\omega_0^2}{\hat{\delta}(\omega,\omega_0)}, \tag{C12}$$

which we expect in view of Eq. (C2) to be equal to $\frac{A_1}{2}e^{\omega_0\beta/2}$ at $\omega = \omega_0$. Table VI and Fig. 11 show that the agreement is excellent and stable as a function of ω. This study adds to our confidence that the Backus-Gilbert method is a viable approach for spectral function reconstruction in lattice QCD.

TABLE VI. The estimator $a_{\rm BG}/T^3$ as defined in Eq. (C12) with $T = 1/128a$ for different values of λ evaluated at $\omega = \omega_0$. The expected value $\frac{A_1}{2}e^{\omega_0\beta/2} = 1.54255\times 10^4$.

λ	$a_{\rm BG}/T^3$
0.25	$1.540(28)\times 10^4$
0.05	$1.536(23)\times 10^4$
0.005	$1.540(20)\times 10^4$

To summarize, the interpretation of $\hat{\rho}_{\rm BG}(\omega)$ in terms of the spectral function is model independent and determined solely by the resolution function $\hat{\delta}(\bar{\omega},\omega)$. The latter in turn depends on the regulating parameter λ, which is chosen to balance good resolution in frequency against the statistical precision of $\hat{\rho}_{\rm BG}(\omega)$. Prior knowledge on the spectral function, such as the existence of a sharp excitation, can be used *a posteriori* to extract its amplitude in the correlator.

APPENDIX D: LATTICE CORRELATION FUNCTIONS

TABLE VII. Renormalized correlation function $G_A(x_0, T, \mathbf{p}_n)/T^3$. All errors quoted are statistical.

x_0/a	$n=0$	$n=1$	$n=2$	$n=3$	$n=4$	$n=5$
0	$2.9921(9)\times10^{3}$	$2.9962(9)\times10^{3}$	$3.0079(9)\times10^{3}$	$3.0260(9)\times10^{3}$	$3.0496(9)\times10^{3}$	$3.0774(9)\times10^{3}$
1	$9.200(5)\times10^{1}$	$9.335(5)\times10^{1}$	$9.698(5)\times10^{1}$	$1.0213(5)\times10^{2}$	$1.0813(5)\times10^{2}$	$1.1447(5)\times10^{2}$
2	$5.65(1)\times10^{0}$	$6.27(1)\times10^{0}$	$7.83(1)\times10^{0}$	$9.77(1)\times10^{0}$	$1.171(1)\times10^{1}$	$1.343(1)\times10^{1}$
3	$1.566(6)\times10^{0}$	$1.903(5)\times10^{0}$	$2.681(5)\times10^{0}$	$3.527(4)\times10^{0}$	$4.222(4)\times10^{0}$	$4.699(5)\times10^{0}$
4	$5.19(5)\times10^{-1}$	$7.10(4)\times10^{-1}$	$1.117(3)\times10^{0}$	$1.491(3)\times10^{0}$	$1.721(3)\times10^{0}$	$1.801(3)\times10^{0}$
5	$4.02(5)\times10^{-1}$	$5.08(4)\times10^{-1}$	$7.11(3)\times10^{-1}$	$8.58(2)\times10^{-1}$	$9.00(2)\times10^{-1}$	$8.59(2)\times10^{-1}$
6	$3.84(5)\times10^{-1}$	$4.34(4)\times10^{-1}$	$5.16(3)\times10^{-1}$	$5.46(2)\times10^{-1}$	$5.14(1)\times10^{-1}$	$4.44(1)\times10^{-1}$
7	$3.77(5)\times10^{-1}$	$3.90(4)\times10^{-1}$	$3.95(3)\times10^{-1}$	$3.64(2)\times10^{-1}$	$3.06(1)\times10^{-1}$	$2.386(7)\times10^{-1}$
8	$3.72(5)\times10^{-1}$	$3.59(4)\times10^{-1}$	$3.16(2)\times10^{-1}$	$2.54(1)\times10^{-1}$	$1.887(9)\times10^{-1}$	$1.319(6)\times10^{-1}$
9	$3.68(5)\times10^{-1}$	$3.37(4)\times10^{-1}$	$2.64(2)\times10^{-1}$	$1.85(1)\times10^{-1}$	$1.217(8)\times10^{-1}$	$7.55(5)\times10^{-2}$
10	$3.66(5)\times10^{-1}$	$3.23(4)\times10^{-1}$	$2.30(2)\times10^{-1}$	$1.44(1)\times10^{-1}$	$8.35(8)\times10^{-2}$	$4.59(5)\times10^{-2}$
11	$3.65(5)\times10^{-1}$	$3.15(4)\times10^{-1}$	$2.11(2)\times10^{-1}$	$1.21(1)\times10^{-1}$	$6.37(7)\times10^{-2}$	$3.11(5)\times10^{-2}$
12	$3.65(5)\times10^{-1}$	$3.13(4)\times10^{-1}$	$2.06(2)\times10^{-1}$	$1.14(1)\times10^{-1}$	$5.77(8)\times10^{-2}$	$2.67(6)\times10^{-2}$

[1] E. L. Bratkovskaya, Phenomenology of photon and dilepton production in relativistic nuclear collisions, Nucl. Phys. **A931**, 194 (2014).

[2] L. Ruan, The low and intermediate mass dilepton and photon results, Nucl. Phys. **A931**, 185 (2014).

[3] A. Bazavov *et al.* (HotQCD Collaboration), Fluctuations and correlations of net baryon number, electric charge, and strangeness: a comparison of lattice QCD results with the hadron resonance gas model, Phys. Rev. D **86**, 034509 (2012).

[4] S. Borsányi, Z. Fodor, C. Hoelbling, S. D. Katz, S. Krieg, and K. K. Szabó, Full result for the QCD equation of state with $2+1$ flavors, Phys. Lett. B **730**, 99 (2014).

[5] S. Borsányi, Z. Fodor, S. D. Katz, S. Krieg, C. Ratti, and K. Szabó, Fluctuations of conserved charges at finite temperature from lattice QCD, J. High Energy Phys. 01 (2012) 138.

[6] P. Braun-Munzinger, B. Friman, F. Karsch, K. Redlich, and V. Skokov, Net-charge probability distributions in heavy ion collisions at chemical freeze-out, Nucl. Phys. **A880**, 48 (2012).

[7] J Stachel, A Andronic, P Braun-Munzinger, and K Redlich, Confronting LHC data with the statistical hadronization model, J. Phys. Conf. Ser. **509**, 012019 (2014).

[8] B. B. Brandt, A. Francis, H. B. Meyer, and D. Robaina, Chiral dynamics in the low-temperature phase of QCD, Phys. Rev. D **90**, 054509 (2014).

[9] R. D. Pisarski and M. Tytgat, Propagation of cool pions, Phys. Rev. D **54**, R2989 (1996).

[10] D. T. Son and M. A. Stephanov, Pion propagation near the QCD chiral phase transition, Phys. Rev. Lett. **88**, 202302 (2002).

[11] D. T. Son and M. A. Stephanov, Real-time pion propagation in finite-temperature QCD, Phys. Rev. D **66**, 076011 (2002).

[12] G. Backus and F. Gilbert, The resolving power of gross earth data, Geophys. J. R. Astron. Soc. **16**, 169 (1968).

[13] G. Backus and F. Gilbert, Uniqueness in the inversion of inaccurate gross earth data, Phil. Trans. R. Soc. A **266**, 123 (1970).

[14] W. H. Press, S. A. Teukolsky, W. T. Vetterling, and B. P. Flannery, *Numerical Recipes: The Art of Scientific Computing* (Cambridge University Press, Cambridge, England, 2007).

[15] H. Haarioa and E. Somersalo, The Backus-Gilbert method revisited: background, implementation and examples, Numer. Funct. Anal. Optim. **9**, 917 (1987).

[16] B. Schomburg and G. Berendt, On the convergence of the Backus-Gilbert algorithm, Inverse Probl. **3**, 341 (1987).

[17] A. Kirsch, B. Schomburg, and G. Berendt, The Backus-Gilbert method, Inverse Probl. **4**, 771 (1988).

[18] H. B. Meyer, Transport properties of the quark-gluon plasma: a lattice QCD perspective, Eur. Phys. J. A **47**, 86 (2011).

[19] G. Aarts and J. M. Martinez Resco, Continuum and lattice meson spectral functions at nonzero momentum and high temperature, Nucl. Phys. **B726**, 93 (2005).

[20] M. Davier, A. Hocker, and Z. Zhang, The physics of hadronic tau decays, Rev. Mod. Phys. **78**, 1043 (2006).

[21] K. G. Wilson, Confinement of quarks, Phys. Rev. D **10**, 2445 (1974).
[22] K. Jansen and R. Sommer (ALPHA Collaboration), O(a) improvement of lattice QCD with two flavors of Wilson quarks, Nucl. Phys. **B530**, 185 (1998).
[23] M. Hasenbusch, Speeding up the hybrid Monte Carlo algorithm for dynamical fermions, Phys. Lett. B **519**, 177 (2001).
[24] M. Marinkovic and S. Schaefer, Comparison of the mass preconditioned HMC and the DD-HMC algorithm for two-flavour QCD, *Proc. Sci.*, LATTICE2010 (2010) 031, arXiv:1011.0911.
[25] http://luscher.web.cern.ch/luscher/DD-HMC/index.html.
[26] P. Fritzsch, F. Knechtli, B. Leder, M. Marinkovic, S. Schaefer, R. Sommer, and F. Virotta, The strange quark mass and Lambda parameter of two flavor QCD, Nucl. Phys. **B865**, 397 (2012).
[27] M. Bochicchio, L. Maiani, G. Martinelli, G. Rossi, and M. Testa, Chiral symmetry on the lattice with Wilson fermions, Nucl. Phys. **B262**, 331 (1985).
[28] M. Luscher, S. Sint, R. Sommer, P. Weisz, and U. Wolff, Nonperturbative O(a) improvement of lattice QCD, Nucl. Phys. **B491**, 323 (1997).
[29] M. Guagnelli, R. Petronzio, J. Rolf, S. Sint, R. Sommer, and U. Wolff (ALPHA Collaboration), Nonperturbative results for the coefficients b_m and $b_a - b_P$ in O(a) improved lattice QCD, Nucl. Phys. **B595**, 44 (2001).
[30] M. Della Morte, R. Hoffmann, and R. Sommer, Non-perturbative improvement of the axial current for dynamical Wilson fermions, J. High Energy Phys. 03 (2005) 029.
[31] G. P. Engel, L. Giusti, S. Lottini, and R. Sommer, Spectral density of the Dirac operator in two-flavor QCD, Phys. Rev. D **91**, 054505 (2015).
[32] B. B. Brandt, A. Francis, H. B. Meyer, O. Philipsen, and H. Wittig, QCD thermodynamics with O(a) improved Wilson fermions at $N_f = 2$, *Proc. Sci.*, LATTICE2013 (2013) 162, arXiv:1310.8326.
[33] H. B. Meyer, The bulk channel in thermal gauge theories, J. High Energy Phys. 04 (2010) 099.
[34] A. Schenk, Pion propagation at finite temperature, Phys. Rev. D **47**, 5138 (1993).
[35] D. Toublan, Pion dynamics at finite temperature, Phys. Rev. D **56**, 5629 (1997).
[36] H. B. Meyer, A calculation of the bulk viscosity in SU(3) gluodynamics, Phys. Rev. Lett. **100**, 162001 (2008).